



Phase evolution and conductivity study of doped gadolinium-based perovskite oxides

AMIT SINHA

Powder Metallurgy Division, Materials Group, Bhabha Atomic Research Centre, Navi Mumbai 400703, India
For correspondence (amit97@yahoo.com, asinha@barc.gov.in)

MS received 4 August 2021; accepted 5 December 2021

Abstract. The phase evolution and electrical conductivity of strontium-doped gadolinium aluminate (GdAlO_3) based perovskite oxides were investigated. The strontium-doped compositions of GdAlO_3 were prepared through the citrate gel process. Analyses of the phases in the $\text{Gd}_{1-x}\text{Sr}_x\text{AlO}_{3-\delta}$ system were carried out using X-ray diffraction. The morphology of the calcined powders was studied through scanning electron microscopy. The strontium-doped GdAlO_3 powders obtained after calcination at 1000°C was found to be porous agglomerate composed of nanocrystalline grains. The electrical conductivity of $\text{Gd}_{1-x}\text{Sr}_x\text{AlO}_{3-\delta}$ ($x = 0.02\text{--}0.14$) was measured using ac impedance spectroscopy as a function of temperature ranging from 300 to 1000°C under air. The solid solubility of strontium in GdAlO_3 was found to be around 8 mol%. The undissolved strontium precipitated in the form of $\text{SrGd}_2\text{Al}_2\text{O}_7$ phase. The total electrical conductivity of Sr-doped GdAlO_3 increased with increasing amounts of strontium up to 6 mol% doping.

Keywords. Solid oxide fuel cell; oxide ion conductor; impedance spectroscopy; perovskite; citrate gel.

1. Introduction

Fast ion conductors with high oxygen ion conductivity have been attracting considerable technological attention due to their important applications in solid oxide fuel cells (SOFC), oxygen sensors and oxygen permeable membrane catalysts [1–4]. In our previous studies, it was observed that gadolinium aluminate (GdAlO_3) is a potential host system for materials with oxygen ion conductivity [5,6]. Gadolinium aluminate belongs to the family of rare-earth aluminates that crystallize in a slightly distorted orthorhombic perovskite structure. Studies on the Ca-doped GdAlO_3 system showed that the conductivity increases with Ca doping and attains a maximum at 15 mol% doping [6]. The increase in conductivity was attributed to the formation of oxygen vacancies as well as expansion of cell volume due to the greater ionic radius of Ca^{+2} as compared to Gd^{+3} . In the present investigation, the phase evolution and conductivity properties of the strontium-doped GdAlO_3 system were studied. The substitution of strontium for gadolinium is expected to create oxygen vacancies and thereby help in promoting oxygen ion conduction.

2. Experimental

Strontium-doped gadolinium aluminate powders were prepared through a citrate gel route using the same procedure as described elsewhere [5]. This process essentially

involves the complexing of metal nitrate solutions by citric acid followed by the formation of a stable transparent gel by dehydration of the solution. $\text{Gd}(\text{NO}_3)_3 \cdot 6\text{H}_2\text{O}$ (99.99% purity), $\text{Al}(\text{NO}_3)_3 \cdot 9\text{H}_2\text{O}$ (AR Grade) and $\text{Sr}(\text{NO}_3)_2$ (AR Grade) were used as starting materials for preparation of $\text{Gd}_{1-x}\text{Sr}_x\text{AlO}_{3-\delta}$ samples, with $x = 0.02, 0.04, 0.06, 0.08, 0.10, 0.12$ and 0.14 , respectively. The metal ions were complexed by adding sufficient citric acid (AR Grade). The gel obtained after dehydration of solution was slowly dried at 130°C for 2 h that yielded amorphous precursor powder. Initial experiments revealed that phases in Sr-doped GdAlO_3 systems form in the temperature range of $800\text{--}1000^\circ\text{C}$; accordingly, all the doped powders were calcined at 1000°C for 2 h. For phase analysis, powders of the strontium-doped GdAlO_3 were characterized by high-resolution X-ray diffraction using Cu-K_α radiation (Panalytical, Model: X'Pert Pro). The X-ray diffraction (XRD) data were collected at a step interval of 0.01 2θ and a step counting time of 10 s. Theoretical densities of doped compositions were calculated from the lattice parameters derived from XRD data. Rietveld analysis was performed on the XRD data using the Fullprof program incorporated in the WinPLOTR software package [7,8]. Particle size analysis of doped gadolinium aluminate powders was carried out using a particle size analyser (Malvern) using ethanol as dispersing medium.

For the sintering studies, the calcined powders, without further grinding, were compacted in a uniaxial hydraulic

press at 150 MPa. The sintering of green compacts was carried out at 1600°C for 4 h under air. The density of the sintered samples was measured by Archimedes' principle of water displacement as well as by dimensional measurements. The microstructural analysis of the sintered samples was carried out using a field emission microscope (Zeiss DSM982 GEMINI).

Specimens for electrical property measurements were having a dimension of 9–12 mm diameter and 2 mm thickness. The impedance spectroscopy of sintered samples was carried out using a frequency response analyzer (Solartron 1260), which is featured with high input impedance ($>100 \text{ T } \Omega$), a frequency range of 10 μHz to 32 MHz and resolution of 10 μHz . The two electrodes were formed by applying platinum paste (without frit) to the polished surfaces of the sintered pellet and firing at 1000°C. Measurements were carried out under air over a frequency range of 0.1 Hz to 10 MHz in the temperature range of 300 to 1000°C at an ac voltage amplitude of 100 mV. The lead resistance, as obtained by measuring the impedance of a blank cell, was subtracted out from measured impedance values. The corrected impedance was plotted in the complex plane.

3. Results and discussions

3.1 Phase evolution in $\text{Gd}_{1-x}\text{Sr}_x\text{AlO}_{3-\delta}$ system

Figures 1 and 2 show the observed, calculated and difference X-ray powder diffraction patterns of $\text{Gd}_{1-x}\text{Sr}_x\text{AlO}_{3-\delta}$ with $x = 0.02$ and 0.08, respectively. The tick marks below the patterns represent the positions of all possible Bragg reflections. All the peaks could be indexed to orthorhombic crystal structure of GdAlO_3 phase (ICDD PDF 46-0395). The crystal structure was refined based on the structural

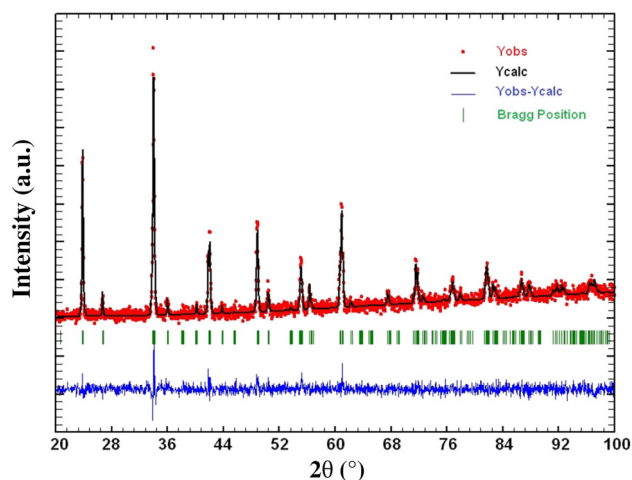


Figure 1. Observed, calculated and difference XRD patterns of $\text{Gd}_{1-x}\text{Sr}_x\text{AlO}_{3-\delta}$ with $x = 0.02$. The tick marks below the pattern represent the positions of all possible Bragg reflections.

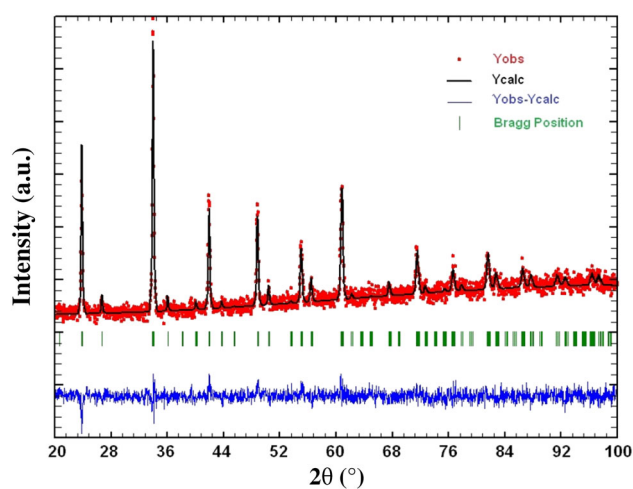


Figure 2. Observed, calculated and difference XRD patterns of $\text{Gd}_{1-x}\text{Sr}_x\text{AlO}_{3-\delta}$ with $x = 0.08$. The tick marks below the pattern represent the positions of all possible Bragg reflections.

data for GdAlO_3 reported previously [9]. Figure 3 shows the XRD patterns of $\text{Gd}_{1-x}\text{Sr}_x\text{AlO}_{3-\delta}$ system with $x = 0.08, 0.10, 0.12$ and 0.14. For the doped powders, with $x > 0.08$, there were additional reflections in the XRD patterns suggesting the presence of a second phase. The additional reflections could be indexed to $\text{SrGd}_2\text{Al}_2\text{O}_7$ phase (ICDD PDF 76-0095). It can be observed that the intensities of peaks corresponding to this second phase increase with the increase in doping level in the range of 10 to 14 mol%, indicating a greater fraction of $\text{SrGd}_2\text{Al}_2\text{O}_7$ phase in the structure with greater Sr doping. The above results suggest that the solubility limit of strontium in GdAlO_3 is ~ 8 mol%.

The variation of lattice parameters of GdAlO_3 doped with strontium is shown in figure 4. With the increase in doping, the lattice parameter ' a ' decreases while ' b ' and ' c ' increase up to a doping level of 8 mol%. With further increase in doping level, the lattice parameters do not change thus obeying Vegard's law [10]. The variation of lattice parameter with Sr doping corroborates the earlier results that the solid solubility of SrO in GdAlO_3 lattice is ~ 8 mol%. The precipitation of $\text{SrGd}_2\text{Al}_2\text{O}_7$ phase at higher strontium doping levels is believed to alter the stoichiometry of GdAlO_3 -based perovskite, making it A-site deficient or B-site excess. The scatter obtained in the lattice parameter values for samples containing Sr doping greater than 8 mol%, may be attributed to the non-stoichiometry of the host lattice.

The quantitative analysis of $\text{SrGd}_2\text{Al}_2\text{O}_7$ present in samples containing strontium more than 8 mol% was carried out by analysing the XRD patterns through the Rietveld refinement program. The expanded portion of observed, calculated and difference X-ray powder diffraction patterns of $\text{Gd}_{1-x}\text{Sr}_x\text{AlO}_{3-\delta}$ with $x = 0.14$ are shown in figure 5. The upper and lower rows of tick marks correspond to the positions of all possible reflections from GdAlO_3 and

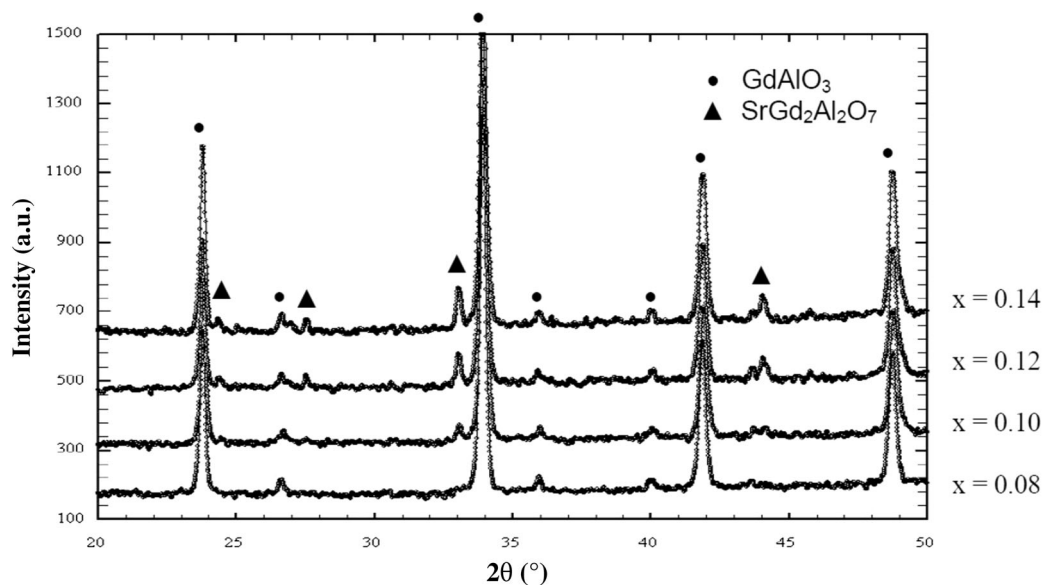


Figure 3. Expanded XRD patterns of $Gd_{1-x}Sr_xAlO_{3-\delta}$ system with $x = 0.08, 0.10, 0.12$ and 0.14 .

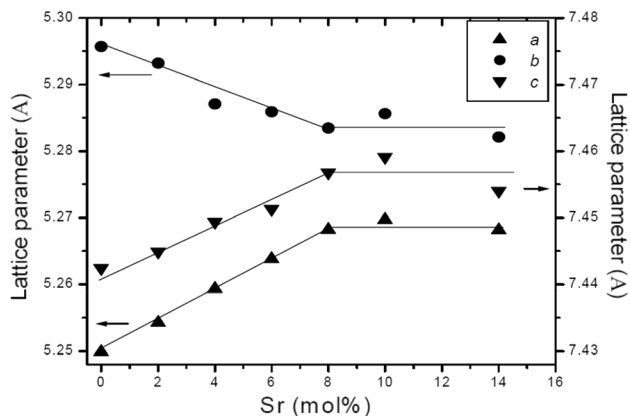


Figure 4. Variation of cell parameters of $Gd_{1-x}Sr_xAlO_{3-\delta}$ as function of strontium content.

$SrGd_2Al_2O_7$ phases, respectively. The results of quantitative phase analysis obtained by Rietveld analysis are shown in table 1. The amount of $SrGd_2Al_2O_7$ was 2 wt% when $x = 0.1$, which increased to 6.83 wt% when strontium doping was increased to $x = 0.14$.

From the Rietveld analysis pattern of $Gd_{1-x}Sr_xAlO_{3-\delta}$ with $x = 0.14$, the crystal structure of $SrGd_2Al_2O_7$ was determined. Figure 6 shows the crystal structure of $SrGd_2Al_2O_7$, which is having lattice parameters $a = 3.70703 \pm 0.00044 \text{ \AA}$ and $c = 19.75449 \pm 0.00422 \text{ \AA}$. These values are very close to the reported lattice parameters of $SrGd_2Al_2O_7$ phase [$a = 3.706(7) \text{ \AA}$ and $c = 19.79(7) \text{ \AA}$] [11]. $SrGd_2Al_2O_7$ belongs to the structural type $Sr_3Ti_2O_7$. In this phase, strontium and gadolinium occupy 12 and 9 coordinated sites, respectively.

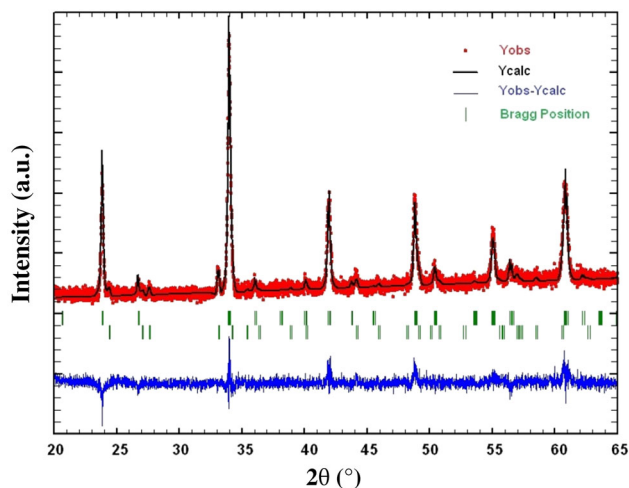


Figure 5. Expanded portion of observed, calculated and difference X-ray powder diffraction patterns of $Gd_{1-x}Sr_xAlO_{3-\delta}$ with $x = 0.14$. The upper and lower rows of tick marks correspond to the positions of all possible reflections from $GdAlO_3$ and $SrGd_2Al_2O_7$ phases, respectively.

Table 1. Phase composition obtained by Rietveld analysis of XRD data of $Gd_{1-x}Sr_xAlO_{3-\delta}$ powders.

Sample code	Sr (mol%)	$SrGd_2Al_2O_7$ content (wt%)
GSA10	10	2.01 (0.49)
GSA12	12	3.00 (0.67)
GSA14	14	6.83 (0.77)

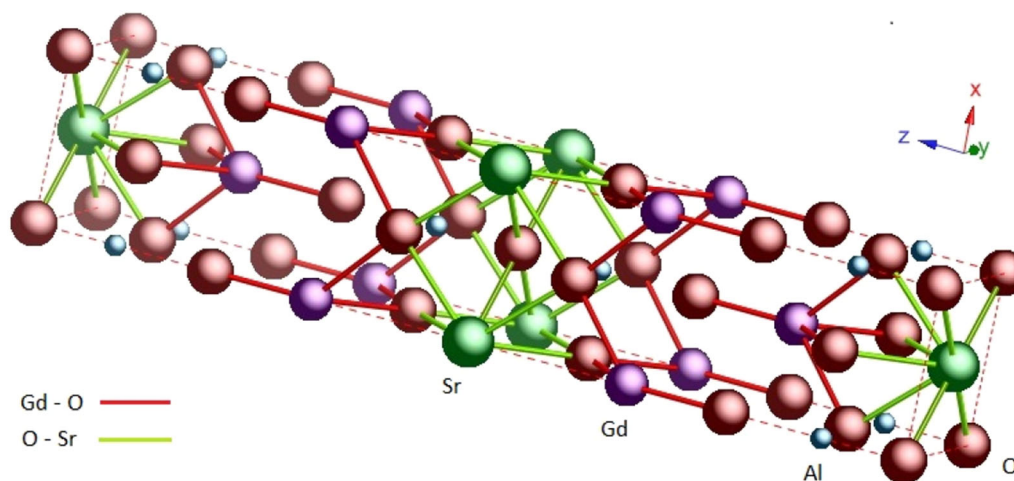


Figure 6. Crystal structure of $\text{SrGd}_2\text{Al}_2\text{O}_7$ obtained by Rietveld analysis of $\text{Gd}_{1-x}\text{Sr}_x\text{AlO}_{3-\delta}$ with $x = 0.14$.

3.2 Sintering study

The variation of sintered density of $\text{Gd}_{1-x}\text{Sr}_x\text{AlO}_{3-\delta}$ system is shown in figure 7. For calculating the theoretical density (TD) of these materials, the crystallographic and structural information (cell volume, solid solubility of Sr in GdAlO_3 phase, percentage of second phase present for $x > 0.08$) obtained from XRD analysis were utilized. It was observed that after sintering at 1600°C for 4 h, the density of $\text{Gd}_{1-x}\text{Sr}_x\text{AlO}_{3-\delta}$ system with $x = 0.02$ – 0.14 , decreased with an increase in Sr doping levels. The sintered density decreased from 97.11% for $x = 0.02$ to $\sim 72\%$ for $x = 0.08$. Within the solid solubility limit, the addition of strontium decreased the sinterability of this material, while the powder processing parameters, calcination and sintering condition remained constant. In the two-phase region, the decrease in sintered density was marginal when the strontium content was increased from 8 to 14 mol%.

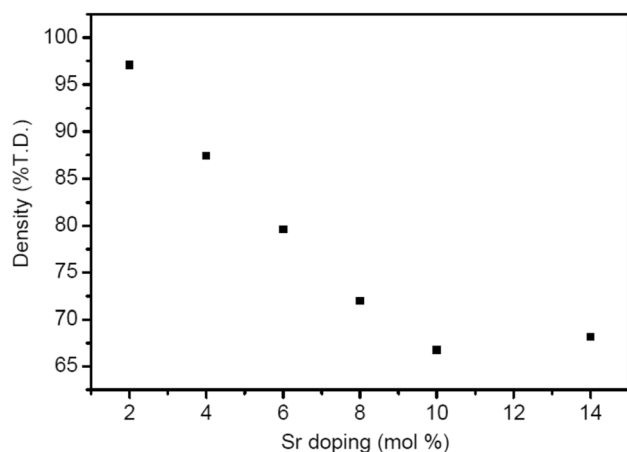


Figure 7. The variation of sintered density of $\text{Gd}_{1-x}\text{Sr}_x\text{AlO}_{3-\delta}$ system.

The low sinterability of rare-earth aluminates doped with strontium has already been reported in the literature [12–14]. In this study, a similar trend in a decrease in sintered density was observed. Systematic decrease in the sintered density with an increase in strontium doping level appear to suggest an increasing fraction of hard agglomerates in the calcined powders that do not break during the initial pressing operation. Micro-pores in these agglomerates may be responsible for low sintered densities in the pellets. To confirm these points, powder particles were characterized by particle size analysis and scanning electron microscopy (SEM).

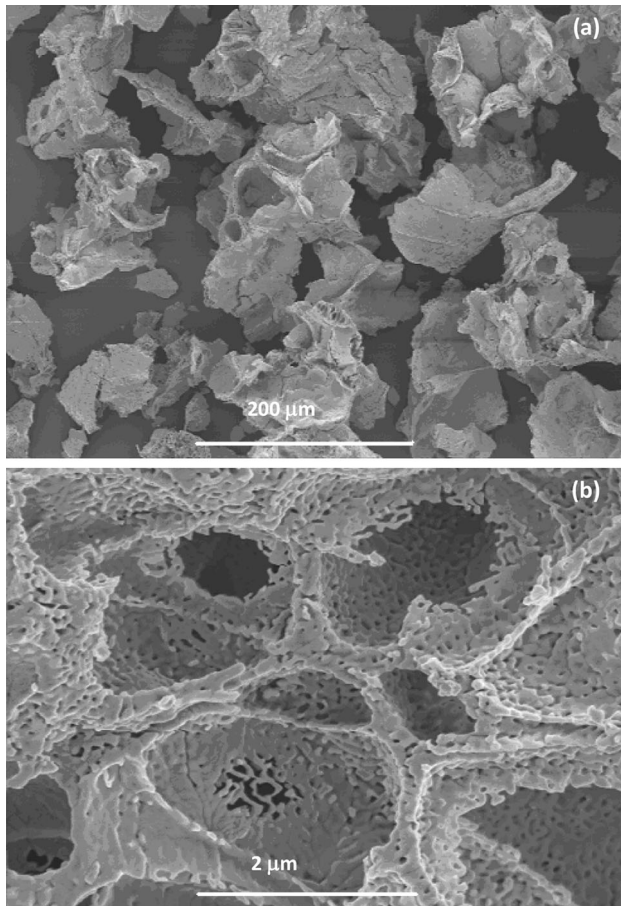
The median powder particle size along with $d_{0.1}$ and $d_{0.9}$ of $\text{Gd}_{1-x}\text{Sr}_x\text{AlO}_{3-\delta}$ (GSA) series of powders are given in table 2. Here, $d_{0.1}$ and $d_{0.9}$ represent particle diameter corresponding to 10 and 90% of the cumulative undersize distribution, respectively. It can be seen that the average particle sizes of all compositions lie in the range of 25–27 μm , whereas that of $d_{0.9}$ lie between 52 and 57 μm , and the values of $d_{0.1}$ are greater than 4 μm . These results indicate that powders are agglomerated, and data presented in table 2 are the agglomerate sizes.

To confirm the agglomeration behaviour of the powder of the GSA series, the morphology of the powder particles was studied through SEM. Though powders of all compositions of this series were studied through SEM, only photomicrographs of GSA02 and GSA08 are shown and discussed in the present text.

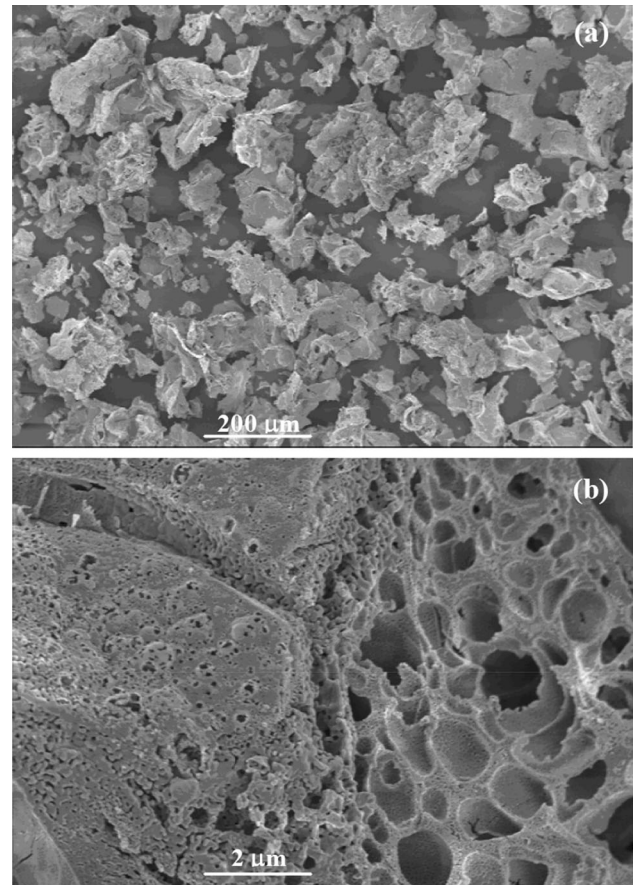
The SEM photomicrographs of GSA02 powder are shown in figure 8. The figures exhibit partially sintered nano-grained powders. The average grain size is less than 25 nm, whereas the average pore size is less than 10 nm. The powder is flaky, having a characteristic shell structure. The shell is porous, indicating the evolution of gases during drying and/or calcination stages. The shell is made up of nano-grains that are partially sintered. The nanopowders/grains have lost their identities. Some

Table 2. Particle size data of $Gd_{1-x}Sr_xAlO_{3-\delta}$ powders calcined at 1000°C for 2 h.

Sr doping (mol%)	Sample code	$d_{0.1}$ (μm)	Median particle size (μm)	$d_{0.9}$ (μm)
2	GSA02	4.16	25.0	52.77
4	GSA04	4.31	25.95	52.99
6	GSA06	4.12	24.23	54.26
8	GSA08	5.38	28.34	59.28
10	GSA10	4.96	26.66	56.85
14	GSA14	4.10	26.71	55.57

**Figure 8.** Scanning electron photomicrographs of GSA02 powder calcined at 1000°C for 2 h.

structures are similar to the formation of dendrites out of molten state. The rupture of nano-grained shell suggests that sintering took place after the evolution of gases. The morphology of powder suggests it would be easily friable; i.e., could be ground easily. The SEM photomicrographs of GSA08 powder are shown in figure 9. The powder is agglomerated and porous, and has a similar characteristic shell structure. The nano-grains in the shell are sintered and in most places lose their particle identity,

**Figure 9.** Scanning electron photomicrographs of GSA08 powder calcined at 1000°C for 2 h.

which makes the shell hard and difficult to crush during compaction state.

3.3 *ac* Impedance spectroscopy of strontium-doped $GdAlO_3$

The Nyquist plots of strontium-doped gadolinium aluminate samples carried out at 300°C are shown in figure 10. The total impedance of $Gd_{1-x}Sr_xAlO_{3-\delta}$ samples

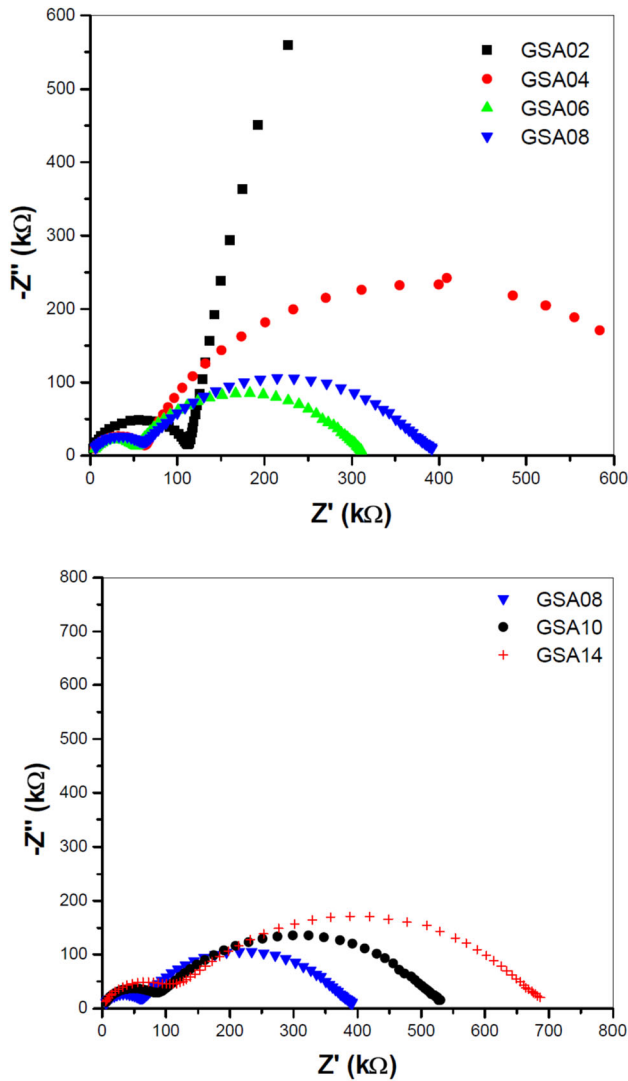
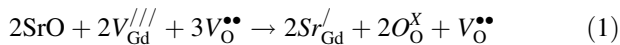


Figure 10. Nyquist plots of $Gd_{1-x}Sr_xAlO_{3-\delta}$ ($x = 0.02$ to 0.14) measured at 300°C . All the data are normalized to $L/A = 0.20$.

decreased with initial strontium doping. The addition of strontium in $GdAlO_3$ creates a vacancy in the oxygen sublattice to compensate for the charge of Sr in the cation sub-lattice (Sr_{Gd}^{\prime}). The point defect reaction can be written:



With the increase in strontium doping up to 6 mol% the total resistance of the sample decreased. The drop in resistivity can be attributed to the formation of oxygen vacancy as well as an increase in the cell volume of the perovskite that assists the mobility of oxygen ions. The increase in cell volume with initial strontium doping is due to 20% larger ionic radius of Sr^{+2} as compared to Gd^{+3} [15]. With still higher doping, the total resistance of the samples increased monotonously. This may be attributed to the formation of secondary phases in $Gd_{1-x}Sr_xAlO_{3-\delta}$

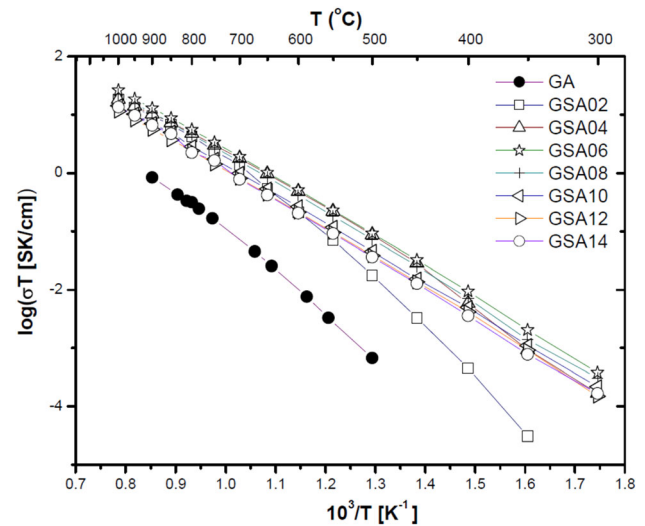


Figure 11. Plots of $\log(\sigma T)$ as a function of inverse of temperature for $Gd_{1-x}Sr_xAlO_{3-\delta}$ system.

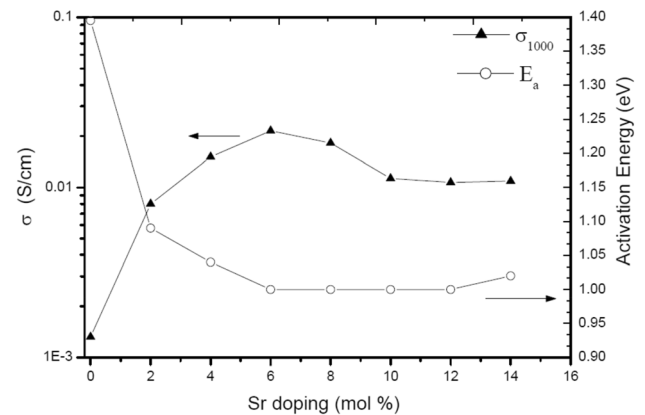


Figure 12. Effect of strontium doping on the total conductivity and activation energy of $Gd_{1-x}Sr_xAlO_{3-\delta}$ system.

system. Similar behaviours have been observed in Ca- and Ba-doped $GdAlO_3$ systems, wherein the presence of secondary phases in specimens with higher Ca/Ba content resulted in a decrease in the overall conductivity of the host system [5,16]. Strontium doping in $GdAlO_3$ contributes to conductivity by the generation of point defects (oxygen vacancy) and associated lattice stretching due to the mismatch of ionic radii between dopant and host ions. This is true as long as the dopant ion is in a solid solution of the host system. At a higher doping level, solubility limit Sr^{+2} is crossed resulting in the formation of precipitate containing the dopant ion. In general, it has been observed that the conductivity of secondary phases is substantially lower than that of the host system.

The plots of $\log(\sigma T)$ as a function of the inverse of temperature for $Gd_{1-x}Sr_xAlO_{3-\delta}$ system are shown in figure 11. The activation energies for conduction were calculated within the temperature range of 400 to 800°C .

Up to 2 mol% Sr doping the conductivity plots exhibited a non-linear behaviour, which may be attributed to changes in the conduction mechanism. Figure 12 shows the effect of strontium doping on total conductivity at 1000°C and activation energy (E_a). With the increase in the Sr doping, the total conductivity of the samples increased. The total conductivity of the strontium-doped samples became maximum at $x = 0.06$. $\text{Gd}_{0.94}\text{Sr}_{0.06}\text{AlO}_{3-\delta}$ exhibited a total conductivity of $\sigma = 0.021 \text{ S cm}^{-1}$ at 1000°C. It may be noted here that the sintered density of 6 mol% doped pellet was only 80% of the theoretical value and hence the conductivity value reported here are under-estimated. The activation energy for conduction decreased with initial strontium doping and became minimum at 6 mol% Sr content. Further doping did not affect the activation energy, which remained almost constant up to 12 mol%. At 14 mol%, a slight increase in activation energy was observed.

4. Conclusions

The solid solubility of strontium in GdAlO_3 was found to be ~ 8 mol%. The larger difference in ionic radii between Gd^{+3} and Sr^{+2} led to a smaller solid solution range as compared to the Ca-doped GdAlO_3 system. At higher strontium content, the undissolved strontium precipitated in the form of $\text{SrGd}_2\text{Al}_2\text{O}_7$ phase. The total electrical conductivity of the Sr-doped GdAlO_3 system increased with increasing amounts of strontium up to 6 mol%. The maximum conductivity was found to be 0.021 S cm^{-1} at 1000°C. This is about $\sim 20\%$ of the conductivity of 8YSZ at the same temperature. As compared with the Ca-doped GdAlO_3 system, the Sr-doped system exhibited a lower total conductivity. However, the sintered density of the present

system was quite low as compared to samples of Ca-doped GdAlO_3 . Because of the lower density, the conductivity values reported here are under-estimated.

References

- [1] Steele B C H and Heinzl A 2001 *Nature* **414** 345
- [2] Singh P and Goodenough J B 2012 *Energy Environ. Sci.* **5** 9626
- [3] Malavasi L, Fisher C A J and Islam M S 2010 *Chem. Soc. Rev.* **39** 4370
- [4] Badwal S P S and Ciacchi F T 2001 *Adv. Mater.* **13** 993
- [5] Sinha A, Sharma B P and Gopalan P 2006 *Electrochim. Acta* **51** 1184
- [6] Sinha A, Näfe H, Sharma B P and Gopalan P 2008 *J. Electrochem. Soc.* **155** B309
- [7] Rietveld H M 1969 *J. Appl. Cryst.* **2** 65
- [8] Roisnel T and Rodríguez-Carvajal J 2000 *Materials Science Forum, Proceedings of the Seventh European Powder Diffraction Conference (EPDIC 7)* p 118
- [9] Sinha A, Sharma B P, Näfe H and Gopalan P 2010 *J. Alloys Compd.* **502** 396
- [10] Vegard L and Dale H 1928 *Zeitschr. Krist.* **67** 148
- [11] Fava J and Flem J L 1975 *Mat. Res. Bull.* **10** 75
- [12] Anderson P S, Marques F M B, Sinclair D C and West A R 1999 *Solid State Ionics* **118** 229
- [13] Nguyen T L, Dokiya M, Wang S, Tagawa H and Hashimoto T 2000 *Solid State Ionics* **130** 229
- [14] Villas-Boas L A and de Souza D P F 2013 *Mater. Res.* **16** 982
- [15] Shannon R D 1976 *Acta Crystallogr. Sect.* **A32** 751
- [16] Sinha A, Sharma B P and Gopalan P 2012 *J. Alloys Compd.* **536** 204